ARTICLE

Chemical Vapor Deposition Synthesis of N-, P-, and Si-Doped Single-Walled Carbon Nanotubes

Jessica Campos-Delgado,[†] Indhira O. Maciel,[‡] David A. Cullen,[§] David J. Smith,[§] Ado Jorio,[‡,⊥] Marcos A. Pimenta,[⊥] Humberto Terrones,[∥] and Mauricio Terrones[∥,▽,*]

[†]Advanced Materials Department, IPICYT, Camino a la Presa San José 2055, Col. Lomas 4a sección, 78216, San Luis Potosí, SLP, Mexico, [‡]Divisão de Metrologia de Materiais, Instituto Nacional de Metrologia, Normalização e Qualidade Industrial (INMETRO), Duque de Caxias, RJ, 25250-020 Brazil, [§]School of Materials and Department of Physics, Arizona State University, Tempe, Arizona 85287, [⊥]Departamento de Física, Universidade Federal de Minas Gerais, Belo Horizonte, MG, 31270-901 Brazil, [∥]Sociedad Mexicana de Nanociencias y Nanotecnología, SOMENANO, Sierra de la Cruz 144, Col. Lomas 4ª sección, C.P. 78216, San Luis Potosí, S.L.P., Mexico, and [▽]The Department of Physics and Mathematics, Division of Science, Arts and Technology, Universidad Iberoamericana, Avenida Prolongación Paseo de la Reforma 880, Santa Fé 012100, DF, Mexico

ABSTRACT Here we report the synthesis of single-walled carbon nanotube bundles by chemical vapor deposition in the presence of electron donor elements (N, P, and Si). In order to introduce each dopant into the graphitic carbon lattice, different precursors containing the doping elements (benzylamine, pyrazine, triphenylphosphine, and methoxytrimethylsilane) were added at various concentrations into ethanol/ferrocene solutions. The synthesized nanotubes and byproduct were characterized by electron microscopy and Raman spectroscopy. Our results reveal intrinsic structural and electronic differences for the N-, P-, and Si- doped nanotubes. These tubes can now be tested for the fabrication of electronic nanodevices, and their performance can be observed.

KEYWORDS: SWNTs · doping · phosphorus · silicon · nitrogen

Tailoring the electronic structure of materials by adding foreign atoms has long been known in the semiconductor industry. The p-type and n-type doping of carbon nanotubes is possible if carbon atoms are substituted with other atomic species containing less or more electrons, respectively. The most common dopants of carbon nanotubes have been boron and nitrogen,[1−10] which are the nearest neighbors of carbon in the periodic table, in groups 13 and 15, respectively.

Nitrogen doping in multi-walled carbon nanotubes (MWNTs) induces the so-called "bamboo-like" morphologies,[5−10] and theoretical calculations of substitutional nitrogen doping in single-walled carbon nanotubes (SWNTs) have revealed a different electronic structure, caused by introducing donor-like features into the conduction band.[6]

The production of N-doped SWNTs has been achieved by arc discharge involving graphite−metal−melamine electrodes[9] and through chemical vapor deposition (CVD)[10] by adding benzylamine to a ferrocene/ethanol solution. In this work, we demonstrate the use of an alternative nitrogen precursor (pyrazine) in order to synthesize N-doped SWNTs, which results in improved nitrogen doping and better quality material.

In the literature, one can also find experimental reports related to phosphorus−nitrogen heterodoping of MWNTs.[11] Theoretically, the substitutional doping of SWNTs by phosphorus is energetically favorable, and experimentally, it has been studied by Raman spectroscopy.[12,13] However, the detailed synthesis and electron microscopy characterization of P-doped SWNTs have not been reported hitherto.

Silicon doping of fullerenes and fullerene-like nanostructures has been achieved experimentally and was reported in the late 1990s.[14,15] The incorporation of silicon species into the hexagonal lattice of SWNTs was proposed theoretically by Baierle *et al.* in 2001.[16] These calculations showed that substitutional Si doping of SWNTs introduces donor-like states above the Fermi level. To the best of our knowledge, the synthesis of Si-doped SWNTs has not been reported.

While electron microscopy and elemental analysis provide direct evaluation of sample morphology and chemical content, respectively, Raman spectroscopy has proven to be a powerful nondestructive tool to characterize SWNTs.[17−19] For example, the radial breathing mode (RBM) signal (~100−400 cm^{-1}) allows the determination of the tube diameter distribution in bundles of SWNTs when different laser lines are used to excite the samples. Interestingly, the morphology of the tangential mode (G band), observed at ~1500−1600 cm^{-1}, changes for metallic

*Address correspondence to mtterrones@gmail.com.

Received for review November 11, 2009 and accepted February 15, 2010.

Published online March 4, 2010. 10.1021/nn901599g

and semiconducting nanotubes. The D band (observed at ~1350 cm^{-1} for E_{laser} = 2.41 eV) appears when the symmetry of the hexagonal network in sp^2-hybridized carbon is broken. Imperfections in the hexagonal lattice, such as defects, dopants, and amorphous-like domains, could thus cause the increment of this band. Recently, the presence of a defect-induced feature (G'_{Def} band) in the immediate vicinity of the second-order G'_{Pris} band (Pris for pristine, located at ~2600−2700 cm^{-1} for E_{laser} = 2.41 eV) has provided valuable information about charged defects present in SWNT structures.[20]

CVD represents a low-cost route to synthesize carbon nanotubes in the presence of metal catalysts, which are responsible for achieving nanotube growth. The production of SWNTs with the floating catalyst method using organometallic compounds (nickelocene ($NiCp_2$), cobaltocene ($CoCp_2$), ferrocene ($FeCp_2$)) stands out as a practical one-step technique to obtain long strands of SWNT bundles.

In this paper, we report the floating catalyst CVD synthesis of N-, P-, and Si-doped SWNTs in the presence of precursors containing such carbon electron donor elements. For nitrogen doping, we compared the use of different precursors (benzylamine and pyrazine) in the resulting N-doped SWNTs. The presence of SWNTs was confirmed in each case by carrying out electron microscopy characterization (SEM and TEM) and by analyzing the RBM signal and other modes using Raman spectroscopy.

Although the expected doping level in our samples is below the detection limit of most elemental analysis techniques (*e.g.*, <1 atom %), we have used the sensitivity of Raman spectroscopy to probe changes in the electronic structure induced by the incorporation of foreign atoms in the hexagonal network *via* the careful inspection of the G′ band spectra of the synthesized materials. The appearance of the G'_{Def} peak, induced by negatively charged defects, and its relative intensity compared to the G'_{Pris} peak ($I_{G'_{Def}}/I_{G'_{Pris}}$) provides insight into the doping atoms within the samples. A detailed comparative analysis indicates the effects of the different dopant atoms on SWNT behavior.

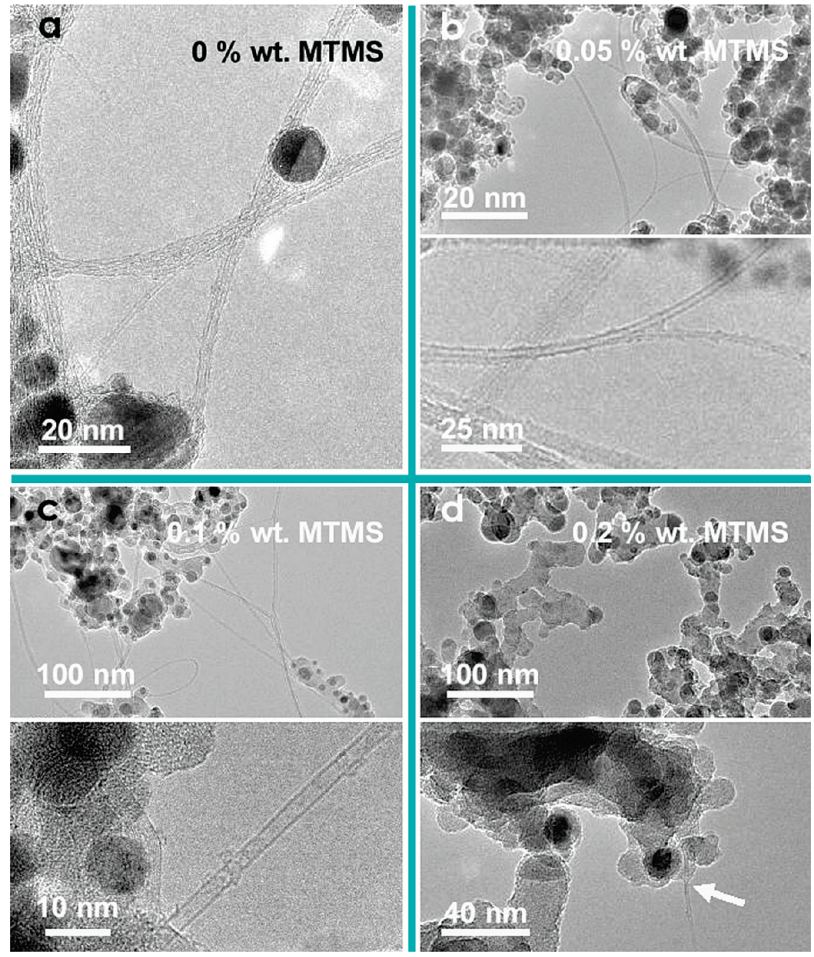

Figure 1. High-resolution transmission electron micrographs of SWNTs produced with different concentrations of methoxytrimethylsilane, (a) pristine SWNTs, (b) 0.05 wt %, (c) 0.1 wt %, and (d) 0.2 wt %; the arrow points to a SWNT embedded in the byproduct. (b−d) Top panels contain low-magnification images, and the bottom panels contain higher magnification images, picturing the carbon nanotubes and the morphology of the accompanying byproduct.

RESULTS AND DISCUSSION

Electron Microscopy Analysis. ***Silicon Doping.*** Experiments with methoxytrimethylsilane (MTMS) resulted in the formation of SWNT bundles mixed with byproduct, which were analyzed to determine their morphology and composition.

Figure 1 shows representative TEM images of the nanostructures produced using MTMS. At the lowest concentration of MTMS (0.05 wt %), catalytic Fe nanoparticles were present, embedded in the SWNT bundles, very similar to the pristine material (see Figure 1a,b). Figure 1c shows the material synthesized at 0.1 wt % of MTMS. The top panel depicts a low-magnification image, and the bottom one is a higher magnification image. Using this MTMS concentration, the SWNTs appear with spherical nanoparticles embedded in a matrix. Our elemental analysis measurements, using EELS and HAADF STEM (high-angle annular dark-field scanning transmission electron microscopy) imaging, confirmed that the spherical nanoparticles were composed purely of iron, embedded in a Si−O−C matrix (see Supporting Information).

A higher concentration of silicon (0.2 wt % of MTMS) promoted the formation of short nanorods composed of Si and O with metallic Fe−Si−O hemispherical tips (see Figure 1d and Supporting Information for composition analysis). In these samples, it was difficult to find

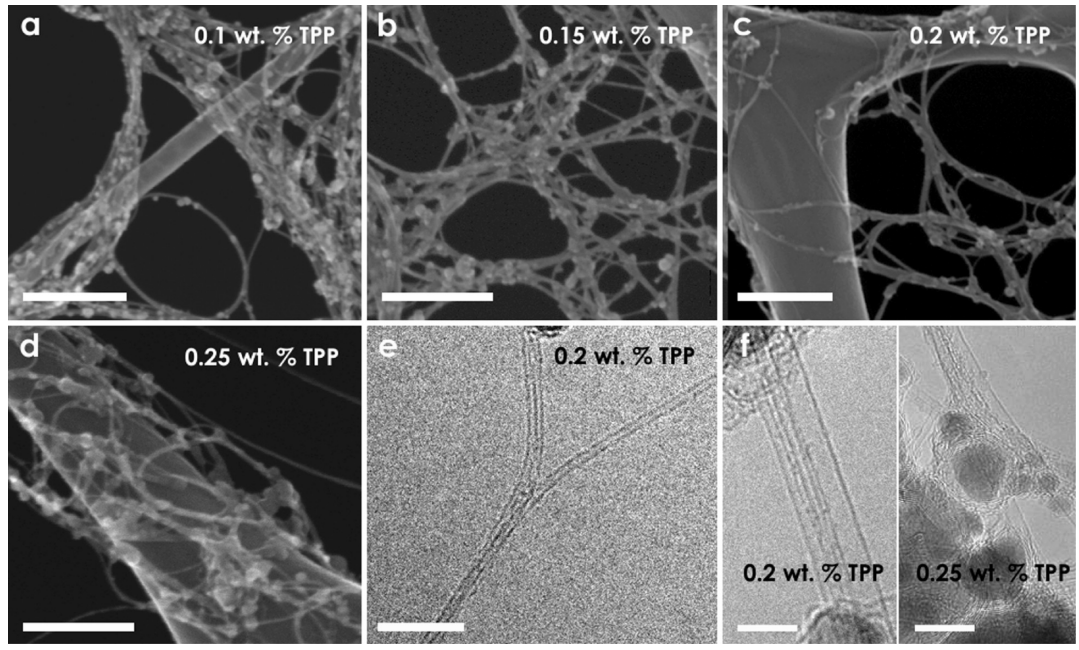

Figure 2. SEM images of SWNTs and byproduct deposited over copper grids synthesized with (a) 0.1, (b) 0.15, (c) 0.2, and (d) 0.25 wt % of TPP; (e) TEM image of the material synthesized with 0.2 wt %, (f) higher resolution TEM images at 0.2 wt % (left panel) and 0.25 wt % (right panel). Scale bars in panels a−d represent 200 nm. Scale bars in panels e and f represent 10 and 5 nm, respectively.

numerous SWNTs; nevertheless, in the bottom panel of Figure 1d, an individual SWNT can be observed along with the byproduct synthesized for this MTMS concentration.

It appears that the formation of pure Fe particles, which serve as SWNT catalysts during growth, was not favored when using these experimental conditions. According to the phase diagram, the formation of binary Fe−Si alloys is highly probable at this synthesis temperature; hence, the catalytic activity of Fe was reduced, and the formation of nanotubes was not abundant.

However, due to the high sensitivity of Raman spectroscopy for identifying SWNTs, their presence was confirmed by the observation of RBM signal (see Figures 4 and 5).

Phosphorus Doping. The introduction of triphenylphosphine (TPP) led to the synthesis of SWNTs and nanoparticles, as depicted in Figure 2. Figure 2a−d displays SEM micrographs of SWNTs produced at 0.1, 0.15, 0.2, and 0.25 wt %, respectively. The nanoparticles accompanying the nanotubes, as observed in Figure 2a−d, are dense when imaged by HAADF STEM (see Supporting Information Figure S7). The high proportion of SWNTs in this sample indicates that mainly Fe was catalyzing their growth. Figures 4 and 5 show Raman spectra analysis of these samples (discussed below).

Nitrogen Doping. The nature and morphology of the materials produced with benzylamine will not be discussed here; the interested reader is referred to ref 10 for microscopy characterization and further details. Briefly, this material contains SWNTs accompanied by Fe nanoparticles. Extensive characterization of these samples using X-ray photoelectron spectroscopy (XPS)[21] has revealed that the synthesized N-doped nanotubes exhibit a maximum concentration at 0.3 atom % of N. EDX or EELS is unable to detect such low concentrations, and Raman characterization thus becomes the most adequate tool to observe the doping effects in SWNTs.

When pyrazine was used as the nitrogen precursor in the N-doped SWNT synthesis, metallic (Fe) nanoparticles were also observed in the samples (see Figure 3a−d). At low pyrazine concentrations, the amount of Fe nanoparticles present in the sample is scarce and it increases gradually with increasing pyrazine concentration in the sprayer solution. Raman results for these samples are discussed in the following section.

Micro-Raman Spectroscopy Analysis. We carried out an RBM evolution study as a function of doping level with spectra recorded at $E_{laser} = 1.96$ eV. In addition, the $I_{G'_{Def}}/I_{G'_{Pris}}$ relative intensities at $E_{laser} = 2.41$ eV were used to determine the effects of doping on the electronic and vibrational structure of SWNTs. It has been theoretically predicted and experimentally demonstrated that the incorporation of heavier elements in the hexagonal carbon lattice is energetically favored in narrower nanotubes that exhibit higher radii of curvature.[12,13,22]

In our experiments, the production of narrower nanotubes when P, N, and Si atoms are substitutionally doping the SWNTs is illustrated in Figure 4. In particular, the RBM region of the Raman spectra recorded at $E_{laser} = 1.96$ eV is plotted for the P-, N-, and Si- doped samples (Figure 4a−c, respectively). The red arrows help to visualize the RBM features that significantly de-

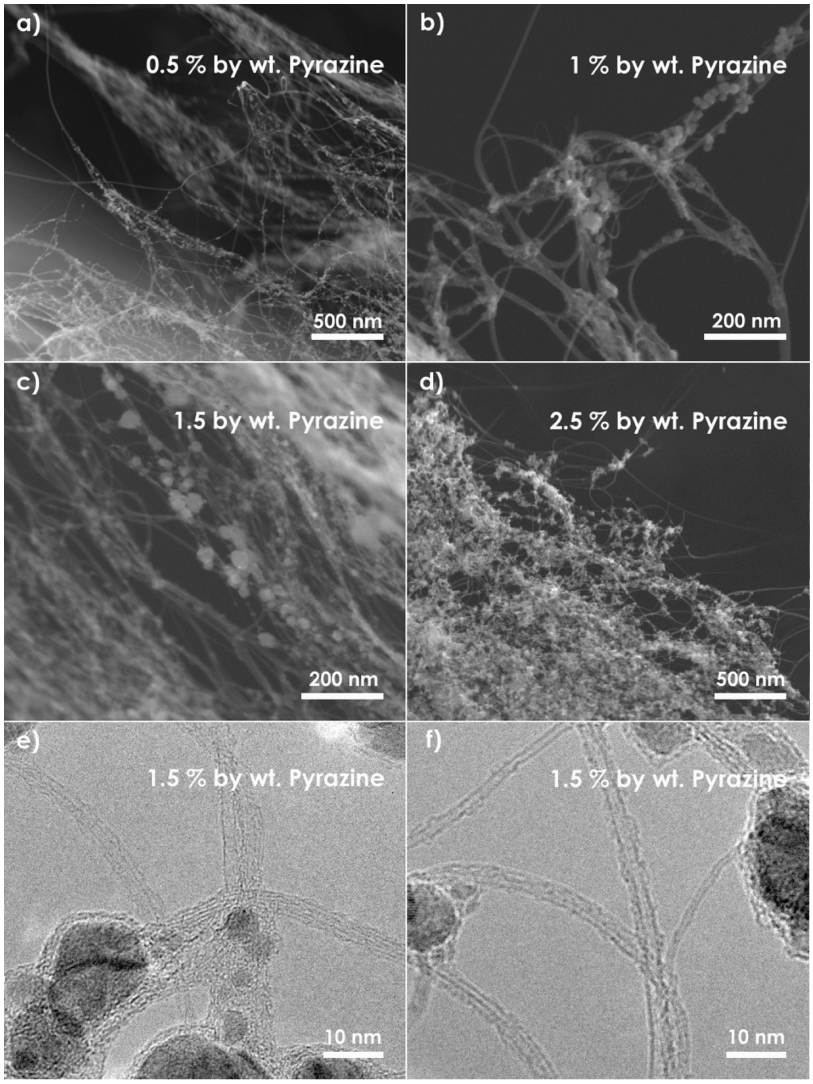

Figure 3. (a−d) SEM images of SWNTs synthesized in the presence of pyrazine at concentrations of 0.5, 1, 1.5, and 2.5 wt %, respectively. (e,f) HRTEM images of the material at 1.5 wt % of pyrazine.

crease in relative intensity as the doping precursor concentration in the ferrocene/ethanol solution is increased. This decrease can be correlated with the absence of large diameter doped SWNTs.

Figure 5a shows a plot of the RBM and G′ band regions, recorded at E_{laser} = 2.41 eV, for the samples synthesized with TPP, pyrazine, benzylamine, and MTMS and of pristine SWNTs annealed at 400 °C (HT Pristine). This plot reveals that SWNTs were successfully grown in the different environments and at every concentration used.

A two-peak Lorentzian fitting of the G′ band of all the spectra shown in Figure 5a was carried out according to previous studies.[13,20,23] This procedure has to be carried out with care because the G'_{Pris} frequency depends on the tube diameter, which changes upon doping (the more doping, the more narrow tubes). The ratio of the relative intensities (amplitudes) of the G'_{Def} band and G'_{Pris} band ($I_{G'_{Def}}/I_{G'_{Pris}}$) was computed, and the resulting values are plotted in Figure 5b as a function of doping atoms available per carbon atom during the synthesis in the precursor ferrocene/ethanol solution. The solid squares represent the set of P-doped samples synthesized with triphenylphosphine; the solid circles and solid triangles represent the N-doped samples synthesized with pyrazine and benzylamine, respectively, and the solid inverse triangles are for the Si-doped materials synthesized using methoxytrimethylsilane as precur-

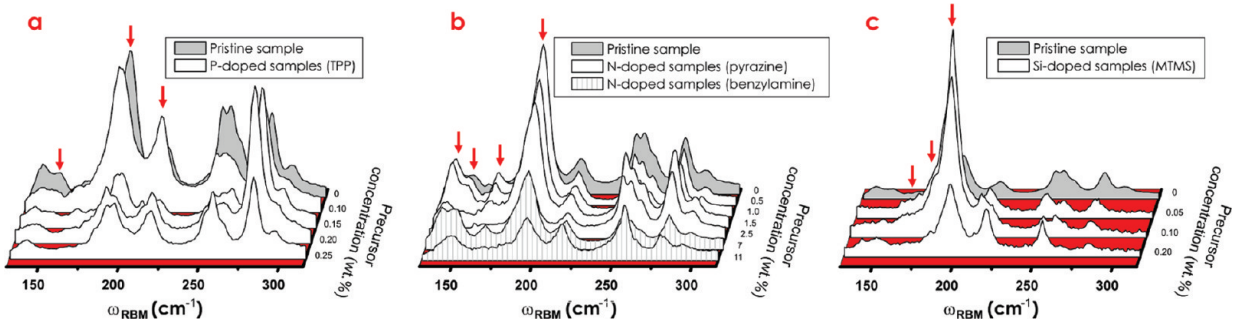

Figure 4. RBM spectra recorded at E_{laser} = 1.96 eV, (a) P-doped SWNTs synthesized with different concentrations of TPP, (b) N-doped SWNTs synthesized with different concentrations of benzylamine and pyrazine, and (c) Si-doped SWNTs synthesized with methoxytrimethylsilane at different concentrations. The spectra were normalized to the G band, and the red arrows point to RBM features that decrease in intensity as the precursor concentration is increased.

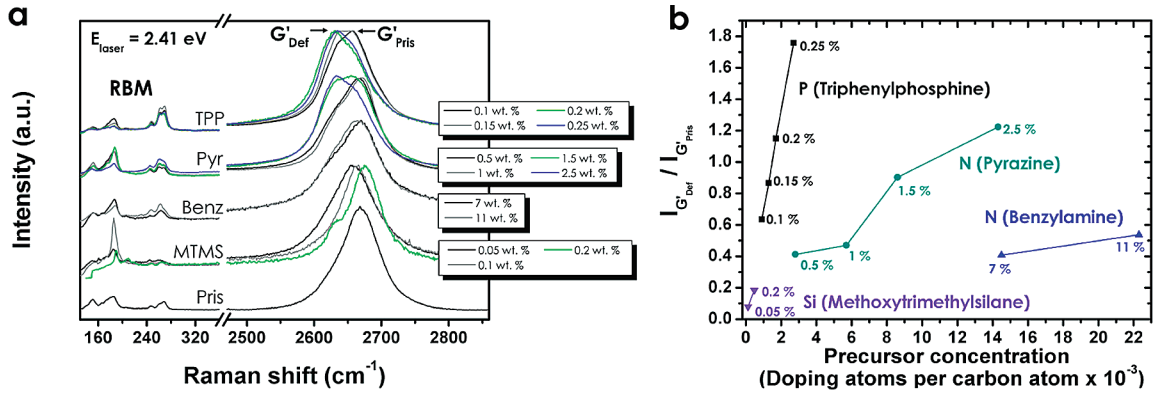

Figure 5. (a) Raman spectra of the synthesized materials normalized to the G′ band, acquired with E_{laser} = 2.41 eV, showing the RBM and G′ band regions. The spectrum of pristine SWNTs annealed at 400 °C as described in ref 13 is included for comparison. (b) Plot of the $I_{G'_{Def}}/I_{G'_{Pris}}$ relative intensities as a function of doping atoms (P, N, and Si) per carbon atoms introduced in the synthesis environment (calculated from the precursor concentration, such concentrations are also included next to each corresponding symbol).

sor. For all precursors, an increase in the number of doping atoms per carbon atom available in the synthesis results in the increase of the $I_{G'_{Def}}/I_{G'_{Pris}}$ relative intensity, thus suggesting the presence of higher doping levels as the precursor concentration increases.

The lowest $I_{G'_{Def}}/I_{G'_{Pris}}$ relative intensity values were obtained for the Si-doped samples. However, these were also the samples with lowest doping atoms per carbon atom. We are confident that higher Si doping will result from the use of higher concentrations of MTMS during the synthesis. However, other experimental conditions should be varied to avoid the suppression of the catalytic effect of Fe when Fe−Si alloys are formed. We believe that the variation of flow rates and temperatures will lead us in the right direction (these experiments are underway).

Although the highest concentration of benzylamine used in this work (11 wt %) provided the highest number of doping atoms per carbon atom during synthesis, the $I_{G'_{Def}}/I_{G'_{Pris}}$ relative intensity values were below those obtained for 1.5 and 2.5 wt % of pyrazine. This demonstrates more efficient N doping when pyrazine was used as the nitrogen precursor. As pointed out earlier, XPS analysis of N-doped SWNTs using benzylamine as the precursor resulted in SWNTs doped with the maximum content of 0.3 atom %. Our Raman results suggest that pyrazine-produced N-doped nanotubes could increase this limit. A careful XPS characterization of our pyrazine N-doped materials is in progress.

Further inspection of Figure 5b leads to the conclusion that the most efficient doping can be attributed to phosphorus because the amount of P atoms available per C atom is relatively small (below the amount of N atoms available) and yet the $I_{G'_{Def}}/I_{G'_{Pris}}$ relative intensity shows its highest values.

However, it is not yet clear whether the $I_{G'_{Def}}/I_{G'_{Pris}}$ relative intensities can be directly compared for different dopants. As discussed in ref 13, different atoms disturb the SWNT lattice differently. In order to address this issue, the samples with highest $I_{G'_{Def}}/I_{G'_{Pris}}$ relative in-

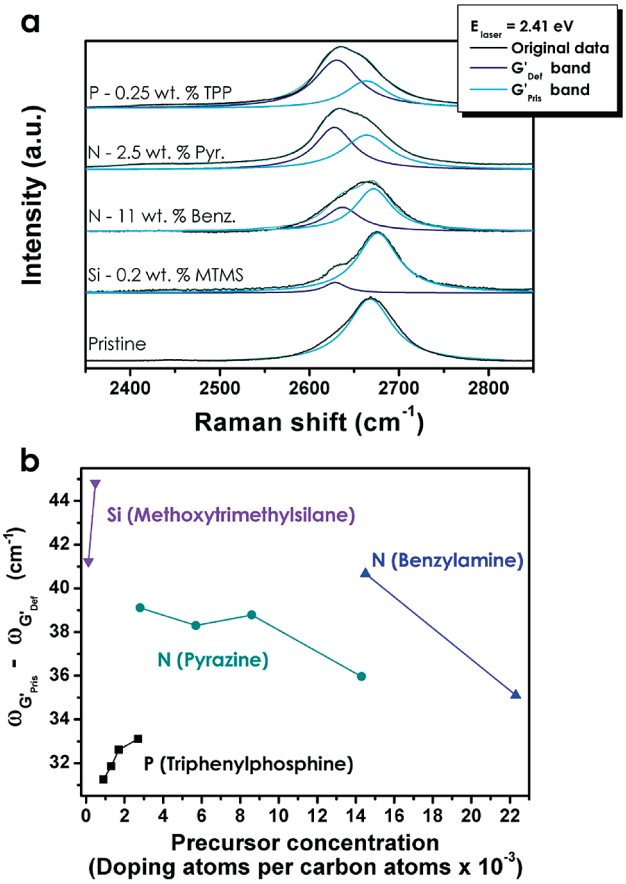

Figure 6. Raman spectra in the G′ band region at E_{laser} = 2.41 eV of the samples with maximum $I_{G'_{Def}}/I_{G'_{Pris}}$ relative intensities for each precursor (corresponding to the highest concentrations used in this work). The blue and cyan lines correspond to the two-peak Lorentzian fitting of the G'_{Def} and G'_{Pris} bands, respectively. The spectrum of annealed pristine SWNTs at 400 °C is included for comparison. (b) Plot corresponding to the G′ band splitting ($\omega_{G'_{Pris}}-\omega_{G'_{Def}}$) as a function of precursor concentration.

tensities from Figure 5b (*i.e.*, 0.25 wt % of TPP, 2.5 wt % of pyrazine, 11 wt % of benzylamine, and 0.2 wt % of MTMS) were selected. The G′ band region and the corresponding two-peak fitting of the above-mentioned samples are depicted in Figure 6a. In this graph, it is very easy to visualize the G'_{Def} bands (blue lines) and the G'_{Pris} bands (cyan lines).

The information of the fitted spectra was further used to calculate the frequency splitting $\omega_{G'_{Pris}} - \omega_{G'_{Def}}$ between the two G′ peaks for the doped samples (see Figure 6b). It is clear from this figure that there is a range of values specific to each doping element. The splitting values for phosphorus are in the range of ~31−33 cm^{-1}, the splitting values for nitrogen are in the range of ~35−40 cm^{-1}, and Si reported the highest values in the range of ~41−45 cm^{-1}. These results suggest that the G′ band splitting is more related to the nature of the doping element rather than to the doping level.

CONCLUSIONS

The synthesis of SWNTs from solutions containing nitrogen, phosphorus, and silicon precursors was carried out *via* aerosol-assisted CVD. Precursors containing the target doping element were mixed in ethanol/ferrocene solutions at different concentrations. Triphenylphosphine was used in the case of phosphorus; methoxytrimethylsilane was used as the silicon precursor, and benzylamine and pyrazine were both used as nitrogen precursors. Electron microscopy studies of the samples as well as RBM Raman signals confirmed the presence of SWNTs in the synthesized materials. Electron microscopy analysis revealed that most of the materials consisted of doped SWNTs entangled with metallic nanoparticles. For Si, unusual morphologies were also observed, such as Si nanorods with metallic tips. As the doping precursor concentration in the sprayer solutions was increased, narrower diameter tubes were favored, according to our RBM analysis. The latter result is consistent with theoretical calculations indicating that dopants of heavier elements embedded in the hexagonal carbon lattice are more energetically favored in narrower tubes exhibiting higher radii of curvature. The $I_{G'_{Def}}/I_{G'_{Pris}}$ relative intensities were used as a direct doping index. Si-doped samples showed low $I_{G'_{Def}}/I_{G'_{Pris}}$ relative intensity values that are directly related to the small amount of silicon atoms available per carbon atoms during the synthesis. Nitrogen doping was more effective when pyrazine was used instead of benzylamine, and phosphorus doping was very effective even at low TPP concentrations. Our Raman results showed that increasing precursor concentration led to higher doping levels, increasing the $I_{G'_{Def}}/I_{G'_{Pris}}$ relative intensities, and that the frequency splitting of the G′ band depended more on the doping element than the doping amount. Further synthesis experiments are being performed in order to have a larger number of samples per doping element, to be able to run Raman spectroscopy measurements, and to elucidate the nature of the G′ band splitting features observed in this work. XPS studies of N-doped SWNTs using benzylamine as a precursor have been carried out recently.[21] These confirm the presence of N within the SWNT material studied here. Additional XPS studies on P-doped, Si-doped, and N-doped using pyrazine SWNTs are currently underway in collaboration with two expert laboratories in order to be able to perform such challenging measurements. Preliminary results reveal the presence of phosphorus in the nanotube lattice (results not shown here).

EXPERIMENTAL SECTION

An aerosol-assisted CVD method with floating catalyst was used, based on ferrocene ($Fe(C_5H_5)_2$) and ethanol (C_2H_5OH) solutions.[24] The doping element was then introduced into the solution by inserting minute amounts of an appropriate compound in order to synthesize the doped SWNTs (such compounds are called precursor compounds in this work). The precursors were chosen based on their physical properties (*i.e.*, melting point and, most of all, solubility in ethanol).

The concentration of ferrocene (as source of catalytic iron) was kept constant at 1.25 wt % for all of the experiments reported here, and the concentration of the precursor was varied. An aerosol of the solution was generated using an ultrasonic sprayer. Argon (or an Ar−H (95/5) mixture) was used as carrier gas inside a quartz tube to direct the aerosol to the hot zone of a tubular furnace operated at 950 °C. After 30 min, the aerosol generator was turned off and the system was allowed to cool to room temperature, and the quartz tube was removed from the furnace. A web-like material containing SWNTs and byproduct was collected from the zone outside the furnace, as illustrated in ref 24.

Nitrogen-doped SWNTs were synthesized reproducing the results reported by Villalpando-Paez and co-workers[10] using benzylamine ($C_7H_7NH_2$) as the N precursor in the ethanol/ferrocene solution at concentrations of 7 and 11 wt %. Another N precursor, namely, pyrazine ($C_4H_4N_2$), was used at concentrations of 0.5, 1, 1.5, and 2.5 wt %.

Phosphorus was inserted into the system using triphenylphos-

TABLE 1. Summary of the Precursor Compounds and Experimental Conditions Used in the Synthesis of N-, P-, and Si-Doped SWNTs

doping element	precursor compound	concentration (wt %)	synthesis temperature	duration	carrier gas	flow rate
N	benzylamine $C_7H_7NH_2$	7, 11	950 °C	30 min	Ar	1.2 L/min
N	pyrazine $C_4H_4N_2$	0.5, 1, 1.5, 2.5	950 °C	30 min	Ar−H_2	1.2 L/min
P	triphenylphosphine $P(C_6H_5)_3$	0.1, 0.15, 0.2, 0.25	950 °C	30 min	Ar−H_2	0.8 L/min
Si	methoxytrimethylsilane $CH_3OSi(CH_3)_3$	0.05, 0.1, 0.2	950 °C	30 min	Ar	0.6 L/min

phine ($P(C_6H_5)_3$) at concentrations of 0.1, 0.15, 0.2, and 0.25 wt %.

The production of SWNTs in the presence of silicon was achieved by adding different concentrations of methoxytrimethylsilane ($CH_3OSi(CH_3)_3$) as a Si precursor. The concentrations used in our experiments were 0.05, 0.1, and 0.2 wt %.

The conditions (temperature, carrier gas, and flow rate) for the different experiments are summarized in Table 1.

Scanning electron microscopy (SEM) characterization was carried out using a XL-30 FEI-SFEG-STEM operated at 10−15 kV. High-resolution transmission electron microscopy (HRTEM) observations were performed with a TECNAI F20 FEI operated at 200 kV and a Phillips CM200 FEG TEM. We also used a JEOL 2010F STEM equipped with a Gatan Enfina spectrometer for recording electron energy loss spectroscopy (EELS).

Micro-Raman spectroscopy measurements were recorded at room temperature using a Renishaw InVia equipment. The spectra were recorded with an Ar line, $\lambda = 514.5$ nm ($E_{laser} = 2.41$ eV), and a He−Ne line, $\lambda = 633$ nm ($E_{laser} = 1.96$ eV), at a power of ~0.3 mW in the backscattering geometry using a 100× objective lens to focus the laser beam. No less than three measurements were recorded per sample, and the spectra shown here are the resulting averages.

Acknowledgment. The authors are thankful to D. Ramírez-González, G. Pérez-Assaf, and K. Gómez-Serrato for technical assistance. This work was supported in part by CONACYT-Mexico Ph.D. Scholarship (J.C.D.). A.J. acknowledges financial support from Rede Nacional de Pesquisa em Nanotubos de Carbono (MCT) and PNPq (Brazil) and AFOSR (USA). M.A.P. acknowledges MCT and Instituto Nacional de Ciencia e Tecnologia de Nanoestruturas de Carbono (Fapemig and CNPq, Brazil).

Supporting Information Available: Information about the chemical composition of the byproduct obtained when MTMS was used at 0.1 and 0.2 wt % is included (HAADF STEM images and EELS spectra). SEM images, bright field, and HAADF STEM images of materials synthesized with TPP are included, which confirm the composition by heavier atoms of the co-products present in the samples. This material is available free of charge *via* the Internet at http://pubs.acs.org.

REFERENCES AND NOTES

1. Han, W.; Bando, Y.; Kurashima, K.; Sato, T. Boron-Doped Carbon Nanotubes Prepared through a Substitution Reaction. *Chem. Phys. Lett.* **1999**, *299*, 368–373.
2. Goldberg, D.; Bando, Y.; Han, W.; Kurashima, K.; Sato, T. Single-Walled B-Doped Carbon, B/N-Doped Carbon and BN Nanotubes Synthesized from Single-Walled Carbon Nanotubes through a Substitution Reaction. *Chem. Phys. Lett.* **1999**, *308*, 337–342.
3. Blase, X.; Charlier, J.-C.; De Vita, A.; Car, R.; Redlich, Ph.; Terrones, M; Hsu, W. K.; Terrones, H.; Carroll, D. L.; Ajayan, P. M. Boron-Mediated Growth of Long Helicity-Selected Carbon Nanotubes. *Phys. Rev. Lett.* **1999**, *83*, 5078–5081.
4. McGuire, K.; Gothard, N.; Gai, P. L.; Dresselhaus, M. S.; Sumanasekera, G.; Rao, A. M. Synthesis and Raman Characterization of Boron-Doped Single-Walled Carbon Nanotubes. *Carbon* **2005**, *43*, 219–227.
5. Sen, R.; Satishkumar, B. C.; Govindaraj, A.; Harikumar, K. R.; Raina, G.; Zhang, J.-P.; Cheetham, A. K.; Rao, C. N. R. B−C−N, C−N and B−N Nanotubes Produced by the Pyrolysis of Precursor Molecules over Co Catalysts. *Chem. Phys. Lett.* **1998**, *287*, 671–676.
6. Terrones, M.; Ajayan, P. M.; Banhart, F.; Blase, X.; Carroll, D. L.; Charlier, J. C.; Czerw, R.; Foley, B.; Grobert, N.; Kamalakaran, R.; *et al.* N-Doping and Coalescence of Carbon Nanotubes: Synthesis and Electronic Properties. *Appl. Phys. A: Mater. Sci. Process.* **2002**, *74*, 355–361.
7. Droppa, R., Jr.; Hammer, P.; Carvalho, A. C. M.; dos Santos, M. C.; Alvarez, F. Incorporation of Nitrogen in Carbon Nanotubes. *J. Non-Cryst. Solids* **2002**, *299*−*302*, 874–879.
8. Glerup, M.; Castignolles, M.; Holzinger, M.; Hug, G.; Loiseau, A.; Bernier, P. Synthesis of Highly Nitrogen-Doped Multi-Walled Carbon Nanotubes. *Chem. Commun.* **2003**, 2542–2543.
9. Glerup, M.; Steinmetz, J.; Samaille, D.; Stéphan, O.; Enouz, S.; Loiseau, A.; Roth, S.; Bernier, P. Synthesis of N-Doped SWNT Using the Arc-Discharge Procedure. *Chem. Phys. Lett.* **2004**, *238*, 193–197.
10. Villalpando-Paez, F.; Zamudio, A.; Elias, A. L.; Son, H.; Barros, E. B.; Chou, S. G.; Kim, Y. A.; Muramatsu, H.; Hayashi, T.; Kong, J.; *et al.* Synthesis and Characterization of Long Strands of Nitrogen-Doped Single-Walled Carbon Nanotubes. *Chem. Phys. Lett.* **2006**, *424*, 345–352.
11. Cruz-Silva, E.; Cullen, D. A.; Gu, L.; Romo-Herrera, J. M.; Muñoz-Sandoval, E.; López-Urías, F.; Sumpter, B. G.; Meunier, V.; Charlier, J.-C.; Smith, D. J.; *et al.* Heterodoped Nanotubes: Theory, Synthesis, and Characterization of Phosphorus−Nitrogen Doped Multiwalled Carbon Nanotubes. *ACS Nano* **2008**, *2*, 441–448.
12. Sumpter, B. G.; Huang, J.; Meunier, V.; Romo-Herrerea, J. M.; Cruz-Silva, E.; Terrones, H.; Terrones, M. A Theoretical and Experimental Study on Manipulating the Structure and Properties of Carbon Nanotubes Using Substitutional Dopants. *Int. J. Quantum Chem.* **2009**, *109*, 97–118.
13. Maciel, I. O.; Campos-Delgado, J.; Cruz-Silva, E.; Pimenta, M. A.; Sumpter, B. G.; Meunier, V.; López-Urías, F.; Muñoz-Sandoval, E.; Terrones, H.; Terrones, M.; *et al.* Synthesis, Electronic Structure, and Raman Scattering of Phosphorus-Doped Single-Wall Carbon Nanotubes. *Nano Lett.* **2009**, *9*, 2267–2272.
14. Kimura, T.; Sugai, T.; Shinohara, H. Production and Characterization of Boron- and Silicon-Doped Carbon Clusters. *Chem. Phys. Lett.* **1996**, *256*, 269–273.
15. Ray, C.; Pellarin, M.; Lermé, J. L.; Vialle, J. L.; Broyer, M.; Blase, X.; Mélinon, P.; Kéghélian, P.; Perez, A. Synthesis and Structure of Silicon-Doped Heterofullerenes. *Phys. Rev. Lett.* **1998**, *80*, 5365.
16. Baierle, R. J.; Fagan, S. B.; Mota, R.; da Silva, A. J. R.; Fazzio, A. Electronic and Structural Properties of Silicon-Doped Carbon Nanotubes. *Phys. Rev. B* **2001**, *64*, 085413.
17. Rao, A. M.; Richter, E.; Bandow, S.; Chase, B.; Eklund, P. C.; Williams, K. A.; Fang, S.; Subbaswamy, K. R.; Menon, M.; Thess, A.; *et al.* Diameter-Selective Raman Scattering from Vibrational Modes in Carbon Nanotubes. *Science* **1997**, *275*, 187–191.
18. Dresselhaus, M. S.; Dresselhaus, G.; Saito, R.; Jorio, A. Raman Spectroscopy of Carbon Nanotubes. *Phys. Rep.* **2005**, *409*, 47.
19. Souza Filho, A. G.; Jorio, A.; Samsonidze, Ge. G.; Dresselhaus, G.; Saito, R.; Dresselhaus, M. S. Raman Spectroscopy for Probing Chemically/Physically Induced Phenomena in Carbon Nanotubes. *Nanotechnology* **2003**, *14*, 1130–1139.
20. Maciel, I. O.; Anderson, N.; Pimenta, M. A.; Hartschuh, A.; Qian, H.; Terrones, M.; Terrones, H.; Campos-Delgado, J.; Rao, A. M.; Novotny, L.; *et al.* Electron and Phonon Renormalization near Charged Defects in Carbon Nanotubes. *Nat. Mater.* **2008**, *7*, 878–883.
21. Elías, A. L.; Ayala, P.; Zamudio, A.; Grobosch, M.; Cruz-Silva, E.; Romo-Herrera, J. M.; Campos-Delgado, J.; Terrones, H.; Pichler, T.; Terrones. M. Spectroscopic Characterization of N-Doped Single-Walled Carbon Nanotube Strands: An XPS and Raman Study. *J. Nanosci. Nanotechnol.* In press.
22. Sumpter, B. G.; Meunier, V.; Romo-Herrera, J. M.; Cruz-Silva, E.; Cullen, D. A.; Terrones, H.; Smith, D. J.; Terrones, M. Nitrogen-Mediated Carbon Nanotube Growth: Diameter Reduction, Metallicity, Bundle Dispersability, and Bamboo-like Structure Formation. *ACS Nano* **2007**, *1*, 369–375.
23. Maciel, I. O.; Pimenta, M. A.; Terrones, M.; Terrones, H.; Campos-Delgado, J.; Jorio, A. The Two Peaks G′ Band in Carbon Nanotubes. *Phys. Status Solidi B* **2008**, *245*, 2197–2200.
24. Lupo, F.; Rodríguez-Manzo, J. A.; Zamudio, A.; Elías, A. L.; Kim, Y. A.; Hayashi, T.; Muramatsu, M.; Kamalakaran, R; Terrones, H.; Endo, M.; *et al.* Pyrolytic Synthesis of Long Strands of Large Diameter Single-Walled Carbon Nanotubes at Atmospheric Pressure in the Absence of Sulphur and Hydrogen. *Chem. Phys. Lett.* **2005**, *410*, 384–390.